

Communication

Chiral Self-Sorting in Truxene-Based Metallacages

Simon Séjourné¹, Antoine Labrunie¹, Clément Dalinot¹, Amina Benchohra¹, Vincent Carré² , Frédéric Aubriet² , Magali Allain¹ , Marc Sallé^{1,*}  and Sébastien Goeb^{1,*} 

¹ Laboratoire MOLTECH-Anjou, UMR CNRS 6200, UNIV Angers, SFR MATRIX, 2 Bd Lavoisier, 49045 Angers CEDEX, France; simon.sejourné@univ-angers.fr (S.S.); antoine.labrunie@univ-angers.fr (A.L.); clement.dalinot@univ-angers.fr (C.D.); amina.benchohra@univ-angers.fr (A.B.); magali.allain@univ-angers.fr (M.A.)

² LCP-A2MC, FR 2843 Institut Jean Barriol de Chimie et Physique Moléculaires et Biomoléculaires, FR 3624 Réseau National de Spectrométrie de Masse FT-ICR à Très Haut Champ, Université de Lorraine, ICPM, 1 boulevard Arago, CEDEX 03, 57078 Metz, France; vincent.carre@univ-lorraine.fr (V.C.); frederic.aubriet@univ-lorraine.fr (F.A.)

* Correspondence: marc.salle@univ-angers.fr (M.S.); sebastien.goeb@univ-angers.fr (S.G.)

Received: 28 November 2019; Accepted: 18 December 2019; Published: 20 December 2019



Abstract: Two chiral face-rotating metalla-assembled polyhedra were constructed upon self-assembling achiral components, i.e., a tritopic ligand based on a truxene core (10,15-dihydro-5H-diindeno [1,2-a;1',2'-c]fluorene) and two different hydroxyquinonato-bridged diruthenium complexes. Both polyhedra were characterized in solution as well as in the solid state by X-ray crystallography. In both cases, the self-sorting process leading to only two homo-chiral enantiomers was governed by non-covalent interactions between both truxene units that faced each other.

Keywords: supramolecular chemistry; self-assembly; self-sorting; metalla-cage; truxene

1. Introduction

Coordination-driven self-assembly methodology has been extensively used during the last few decades to construct bi- or tri-dimensional discrete architecture [1–17]. Beyond the challenge of producing more and more sophisticated compounds, special attention has been given to functional architectures that are responsive to an external stimulus such as light [18–22], redox [23–31], or the addition of a chemical [32] in order to target original properties [33–41]. Those systems are generally achiral and highly symmetric. New synthetic methodologies have therefore been developed to allow for chiral metalla-assembled architecture [5,42–46]. One of these methodologies consists of thermodynamically controlling the self-sorting of multiple building blocks [47–49]. In particular, chiral self-sorting can be spontaneously achieved from a racemic mixture upon metal coordination, leading either to homochiral [50–56] or heterochiral [50,51,57,58] assemblies.

On the other hand, face-rotating polyhedra constitute a recent class of chiral architecture that can be constructed from chiral or achiral linkers and face-rotating component [59–65]. The latter can consist of achiral compounds that exhibit two faces with opposite directionalities such as truxene [62–65], triazatruxene [59,60], and tetraphenylethylene [61]. In particular, the C_{3h} -symmetric hexa-alkylated truxene derivatives exhibit both clockwise (C; green) and anti-clockwise (A; red) faces that are defined by the rotation of the three sp^3 methylene bridges along the C_3 axis (Figure 1a). Upon self-assembly with achiral hydroxyquinonato-bridged diruthenium complexes, the formation of sandwich-type supramolecular cages is expected (Figure 1b). In those cages, the truxene ligands lose their mirror symmetry, thus resulting in several possible stereoisomers. We herein show that through-space interactions between both face-rotating ligands guide the self-assembly process toward only the CC/AA enantiomers couple, whereas the hetero-chiral CA stereoisomer is not observed in this process.

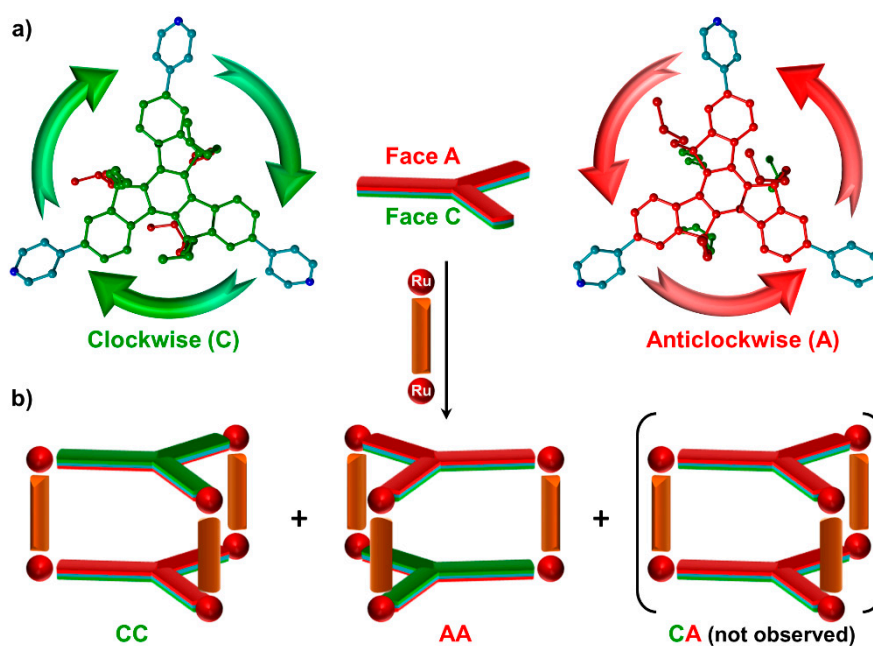
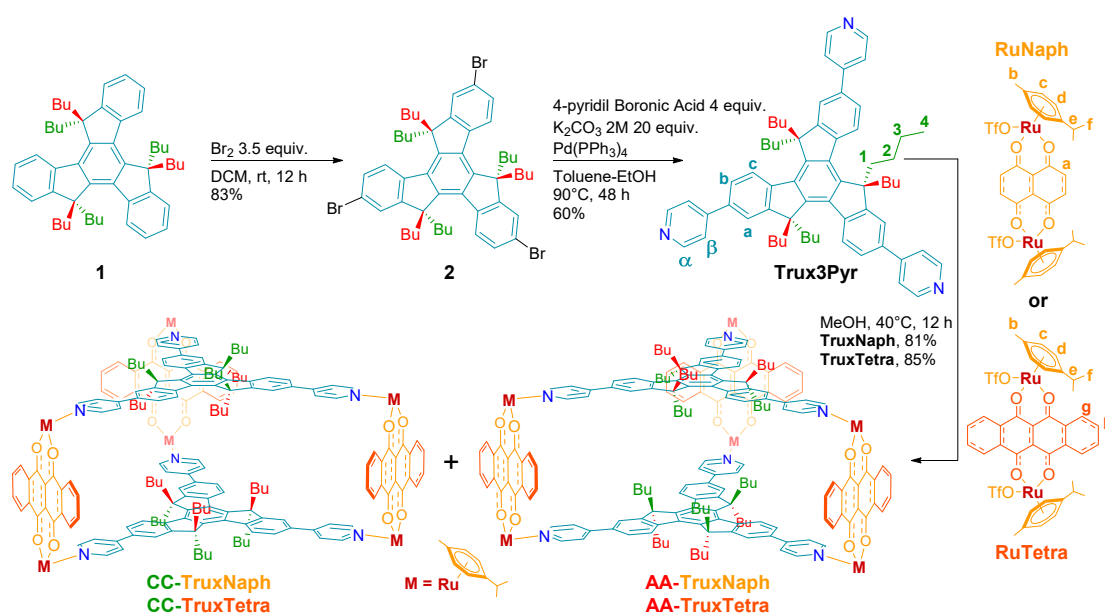


Figure 1. (a) Truxene-based ligand (X-ray) presenting two rotational faces (clockwise (C), green face, and anticlockwise (A), red face) and (b) the three possible metalla-cage structures obtained upon self-assembling with bis-ruthenium complexes.

2. Results and Discussion

The **Trux3Pyr** ligand was synthesized in two steps from hexabutyl truxene derivative **1** in a good yield (Scheme 1) through the adaptation of described procedures [66–68]. Butyl chains were selected to ensure the good solubility of the target ligand and to prevent aggregation. The first step consisted of the regioselective tri-bromination of the truxene core in the presence of Br_2 , thus affording compound **2** in an 83% yield. The target **Trux3pyr** ligand was then obtained in a 60% yield after purification through a palladium-catalyzed Suzuki–Miyaura cross-coupling reaction with 4-pyridinylboronic acid (Figures S3–S9).



Scheme 1. Synthesis of the **Trux3Pyr** ligand and the **CC-TruxNaph**, **AA-TruxNaph**, **CC-TruxTetra**, and **AA-TruxTetra** metalla-cages.

Single crystals of the **Trux3Pyr** ligand that were suitable for X-ray analyses were obtained by the slow evaporation of a $\text{CH}_2\text{Cl}_2/n$ -hexane solution, and the corresponding solid-state crystal structure is depicted in Figure 2. Thanks to the planar geometry of the central truxene core, the three peripheral nitrogen were found to be in the same plane. The pyridine moieties are twisted around the $\text{C}_{\text{trux}}\text{-C}_{\text{pyr}}$ axis with an average angle of $40.8(1)^\circ$, thus minimizing H–H interactions, as reported for similar compounds [69]. An angle of 120° was found between each pyridine axis in accordance with the C_3 symmetry of the **Trux3Pyr** ligand. It was found that the alkyl chains tend to lie away perpendicularly to the truxene plane.

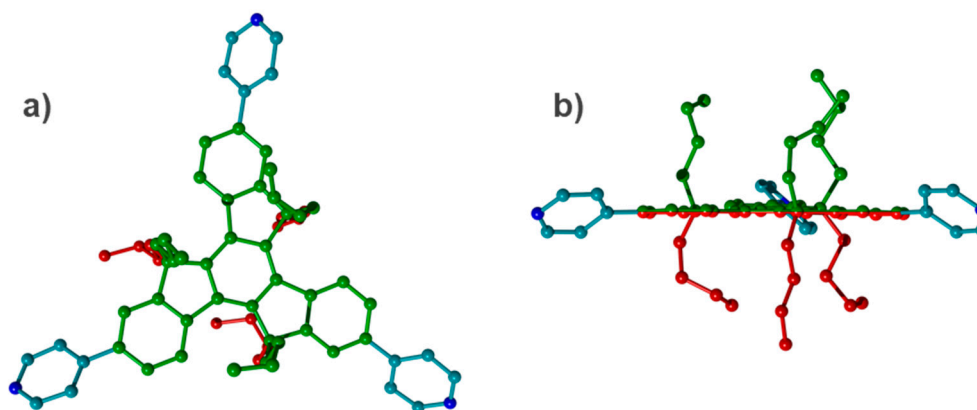


Figure 2. X-ray crystal structure of **Trux3Pyr**: (a) top view (clockwise face in green) and (b) lateral view showing both rotating faces (clockwise in green and anticlockwise in red).

The self-assembly processes between the face-rotating **Trux3Pyr** ligand (two equivalents) and the bis-ruthenium acceptors (three equivalents), **RuNaph** or **RuTetra**, were followed by ^1H NMR in MeOD at $C = 3 \times 10^{-3}$ M. These ruthenium complexes were selected for their accessible syntheses, their rigidity, and their intermetallic distance of ca. 8.3 \AA , a value that we considered sufficient for the six alkyl chains to fit inside the cavity. Note that the reaction of **Trux3Pyr** with the smaller oxalate bis-ruthenium complex (Ru–Ru distance: 5.5 \AA) [70] did not converge into a discrete species. After one night at 50°C with the use of **RuNaph** or **RuTetra**, the spectra became symmetrical and well-resolved. The resulting products were then isolated by precipitation with Et_2O . For both samples, high-resolution ESI-FTICR-MS spectrometry experiments were carried out in MeOH at $C = 10^{-4}$ M (Figure 3). The corresponding spectra confirmed an M_6L_2 stoichiometry in both cases, with characteristic multi-charged isotopic patterns localized at $m/z = 789.6516$, 1024.3024 , and 1415.3877 (main contributions, Figure S16) and at $m/z = 849.6704$, 1099.3257 , and 1515.4192 (main contributions, Figure S17) for the compounds isolated from the reaction of **Trux3Pyr** with **RuNaph** and with **RuTetra**, respectively.

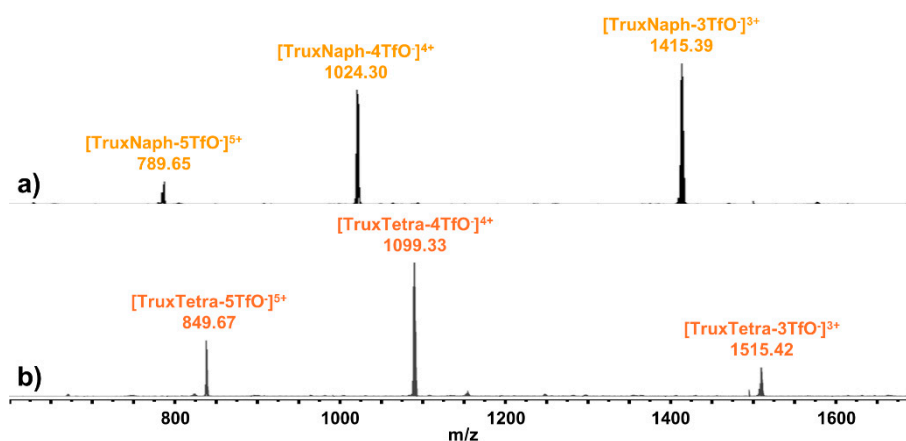


Figure 3. ESI-FTICR mass spectra recorded in MeOH ($C = 10^{-4}$ M) of: (a) **TruxNaph** and (b) **TruxTetra**.

The ^1H NMR, ^1H COSY NMR and ^1H DOSY NMR spectra of both self-assembled cages are shown in Figure 4 and Figures S10–S15. Both the **TruxNaph** and **TruxTetra** ^1H DOSY spectra exhibited only one set of signals, with D values of 2.99 and $2.85 \times 10^{-10} \text{ m}^2 \cdot \text{s}^{-1}$, respectively, meaning that they had similar sizes. The corresponding hydrodynamic radii estimated from the Stokes–Einstein equation [71] were found to be 13 and 14 Å ($T = 298 \text{ K}$). As expected, these values were much larger than the one calculated for the **Trux3Pyr** ligand ($D = 4.78 \times 10^{-10} \text{ m}^2 \cdot \text{s}^{-1}$, MeOD, $R = 8 \text{ Å}$, Figure S9) and were in good agreement with the formation of M_6L_2 self-assemblies. Compared to the **Trux3Pyr** ligand, both isolated discrete assemblies showed upfield shifted H_α and H_β protons after coordination to the ruthenium complex (Figure 4), with chemical shifts in accordance with reported values [72]. Each ^1H NMR spectrum revealed only one set of signals for all **Trux3Pyr** protons (H_α , H_β , H_a , H_b and H_c), this indicating the absence of a mixture of diastereoisomers. Therefore, the reaction between the **Trux3Pyr** ligand and the bis-ruthenium complexes afforded either a mixture of D_3 symmetric CC and AA enantiomers or the C_3 symmetric CA (or AC) stereoisomer alone. This selectivity suggests that a through-space communication existed between both facing panels and orientated the self-assembly process through a chiral self-sorting. This behavior can be compared to what is reported for, e.g., chiral helicates, for which a strong mechanical coupling between the metal units orientates the self-assembly process [43,73]. Additional 2D COSY experiments (Figures S11 and S14) allowed for the assignation of all butyl chains protons. One should note that those located on carbons 1, 2 and 3 of the starting **Trux3Pyr** ligand (see Scheme 1) are diastereotopic [74], two different signals being therefore observed for each methylene group, as illustrated in Figures S1, S3 and S7. In the case of the **TruxNaph** and **TruxTetra** cages, two sets of butyl chains were observed, i.e., those pointing outside the cavity and those pointing inside, more shielded [8], therefore generating 12 signals for the protons located on carbons 1, 2 and 3 (Figure 4d).

Single crystals were obtained for both self-assemblies from the slow diffusion of methyl *tert*-butyl ether in solutions of **TruxNaph** and **TruxTetra** in MeOH. In each case, several crystals were analyzed and gave the same result (Figure 5). Both complexes crystallized in non-centrosymmetric trigonal chiral space groups, $\text{P}3_121$ and $\text{P}3_221$, respectively, for **TruxNaph** and **TruxTetra**, and exhibited very large unit cells volume of ca. $23,500 \text{ Å}^3$. Their Flack parameters were of 0.20 and 0.42, which indicated enantio-enriched crystals. An analysis of the crystal structures gave evidence of chiral self-sorting along the self-assembly process, since only AA and CC enantiomers were present in the solid state. Both self-assemblies exhibited a similar geometric arrangement, organized from two approximatively planar truxene moieties that faced each other. Contrary to what is usually observed for similar metalla-cages in which the two facing polyaromatic ligands tend to get closer to maximize the pi–pi interactions and structure compactness thanks to a large tilt of the lateral ruthenium-based panels [75,76], the six butyl chains present inside the cavity of **TruxNaph** and **TruxTetra** maintained, in this case, both truxene moieties at distances of 7.30 and 7.58 Å, respectively (average value between mean planes). These values were nevertheless smaller than the Ru–Ru distance (8.30 and 8.33 Å) in the bis-ruthenium units of **TruxNaph** and **TruxTetra**, meaning a tilt of the lateral ruthenium side panels of ca. 12° out of the truxene planes. As a consequence, the trigonal prisms were slightly deformed and showed average Bailar twist angles of 7.94 and 8.11° , respectively, (Figure S18) [77]. While the external butyl chains remained nearly linear, those located inside the polyhedra were bent upon confinement within the cavity. Their role was of critical importance in the self-sorting process since they allowed for inter-ligand communication. Indeed, the metalla-prism distortion was minimized when the six butyl chains pointing inside the cavity were alternated. This was the case only for the AA and CC geometries. On the other hand, a self-assembly of two opposite faces (e.g., a CA geometry) would necessitate a much larger tilt of the lateral ruthenium panels in order to preserve the regular alternation, explaining why only the AA and CC enantiomers were observed.

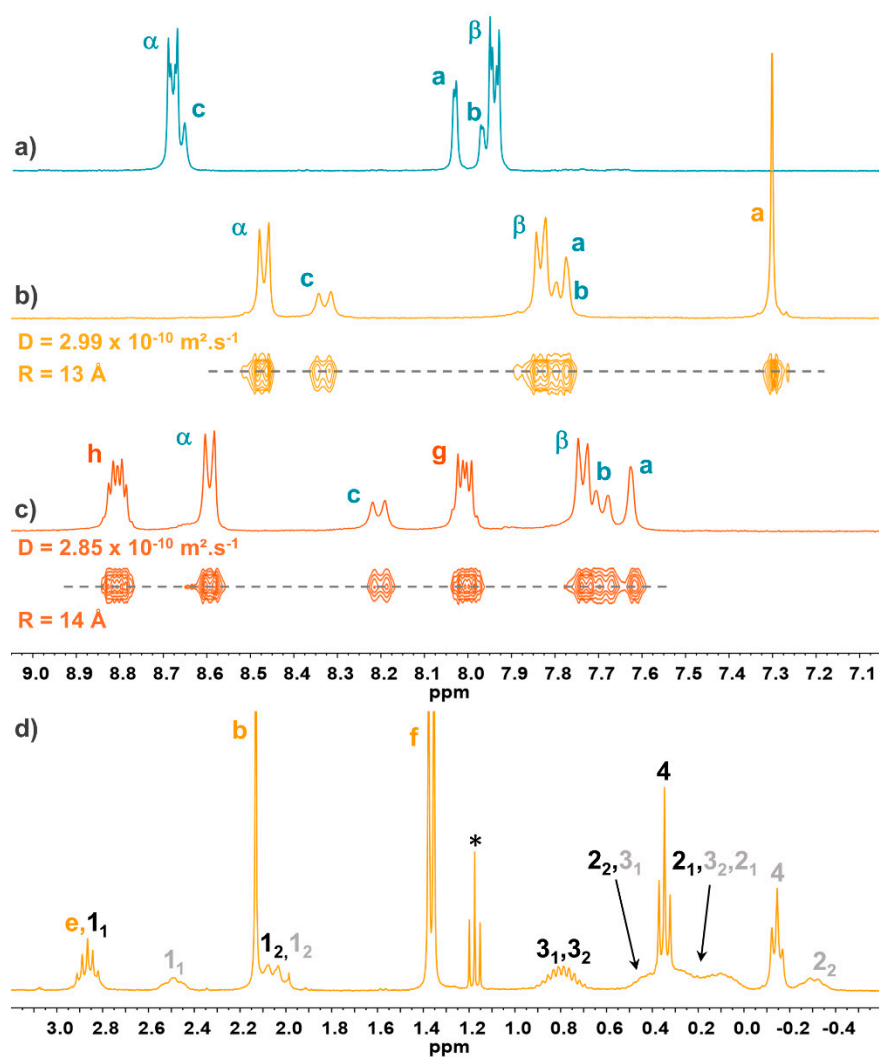


Figure 4. ^1H NMR (298 K, $C = 10^{-3}$ M, MeOG) downfield region of (a) the **Trux3Pyr** ligand, (b) CC- and AA-**TruxNaph**, (c) CC- and AA-**TruxTetra**, and highfield region of (d) CC- and AA-**TruxNaph**. See Scheme 1 for ^1H NMR assignments. Grey and black assignments correspond to the inner cavity and cavity protons, respectively. D corresponds to the diffusion coefficient extracted from an ^1H DOSY NMR experiment, and R to the corresponding hydrodynamic radii calculated from the Stokes–Einstein equation. * Residual Et_2O .

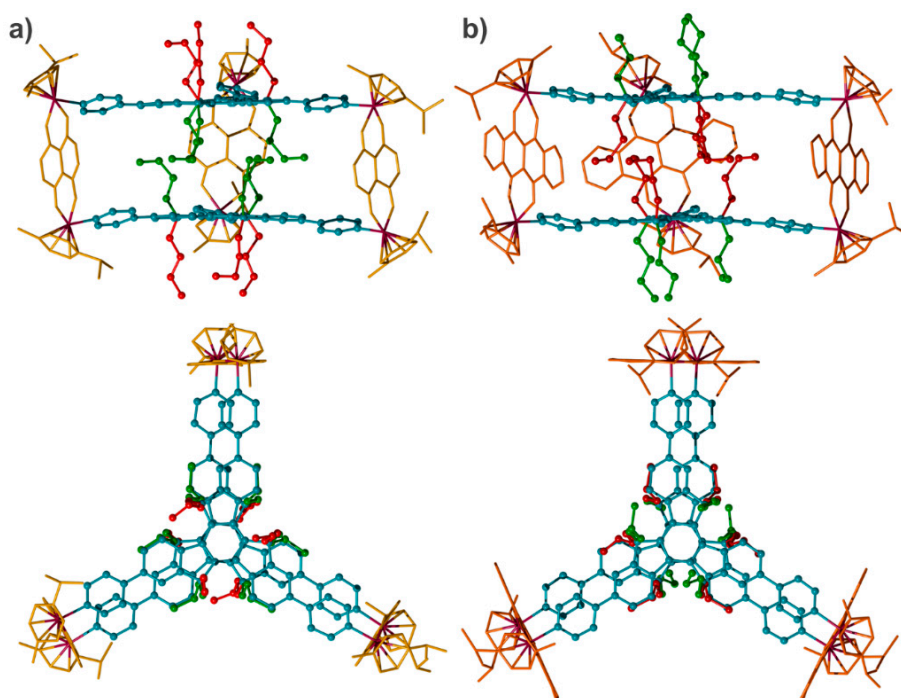


Figure 5. X-ray crystal structures of (a) AA-TruxNaph and (b) CC-TruxTetra.

3. Materials and Methods

3.1. Chemicals

Hexa-alkylated truxene **1** [68], as well as the RuNaph [78] and RuTetra [78] complexes, were synthesized by using procedures described in the literature. All reagents were of commercial reagent grade and were used without further purification. Silica gel chromatography was performed with a SIGMA Aldrich Chemistry SiO₂ (pore size 60 Å, 40–63 μm technical grades) (Sigma-Aldrich, Steinheim, Germany).

3.2. Instrumentation

Characterizations and NMR experiments were carried out on an NMR Bruker Avance III 300 spectrometer or an NMR Bruker Avance III HD 500 spectrometer (Bruker, Wissembourg, France) at 298 K by using perdeuterated solvents. ¹H DOSY NMR spectra were analyzed with the MestReNova software (12.0.1, Mestrelab Research, Santiago de Compostela, Spain). MALDI-TOF-MS spectra were recorded on a MALDI-TOF Bruker Biflex III instrument (Bruker, Wissembourg, France) by using a positive-ion mode. Very high resolution ESI-FTICR mass spectra were performed in positive detection mode on a 7T Solarix 2xR (Bruker Daltonics, Wissembourg, France).

3.3. Experimental Procedure and Characterization Data

2,7,12-tribromo-5,5,10,10,15,15-hexabutyl-10,15-dihydro-5H-diindeno[1,2-a:1',2'-c]fluorene (**2**)

Compound **2** was synthesized after the modification of a reported procedure [68]. Bromine (0.1 mL, 1.94 mmol, 3.5 equivalents) was added to a stirred suspension of truxene **1** (370 mg, 0.545 mmol) in dichloromethane (20 mL) over a 5 min period at room temperature with protection from light. After one night, methanol (50 mL) was added. The resulting precipitate was filtered off and washed with methanol, diethyl ether, and pentane to give compound **2** (412 mg, 0.445 mmol, 83%) as a pale yellow solid. ¹H NMR (500 MHz, 298 K, CDCl₃): δ 8.20 (d, *J* = 8.3 Hz, 3H), 7.57 (d, *J* = 2.1 Hz, 3H), 7.52 (dd, *J* = 8.3 Hz, *J* = 2.1 Hz, 3H), 2.89–2.83 (m, 6H), 2.07–2.01 (m, 6H), 0.98–0.81 (m, 12H), 0.58–0.33 (m, 30H).

^{13}C NMR (126 MHz, CDCl_3) δ 155.89, 145.04, 138.87, 137.71, 129.41, 125.99, 125.61, 121.09, 55.93, 36.50, 26.47, 22.76, and 13.80. HRMS: found: 912.2487; calculated: 912.2480.

Trux3Pyr Ligand

An aqueous solution of K_2CO_3 (0.64 g in 2.5 mL, 4.63 mmol, 20 equivalents) and 4-pyridinylboronic acid (86 mg, 0.699 mmol, 3.2 equivalents) were added to a stirred suspension of **2** (200 mg, 0.218 mmol) in toluene (7 mL) and ethanol (3.5 mL). The mixture was degassed by bubbling argon for 30 min. Then, tetrakis(triphenylphosphine)palladium (0) (70 mg, 0.060 mmol) was added, and the mixture was vigorously stirred and heated to 90 °C. After 48 h, the mixture was cooled to room temperature and extracted with dichloromethane. The organic extracts were washed with water and dried over magnesium sulfate, and then the solvent was evaporated. The residue was purified by chromatography on silica gel by using dichloromethane/ethyl acetate/methanol/triethylamine (from 99/0/0/1 *v/v/v/v* to 47/47/5/1 *v/v/v/v*) to give **Trux3Pyr** (119 mg, 60%) as a pale yellow solid. ^1H NMR (300 MHz, CDCl_3): δ 8.73 (d, J = 8.7 Hz, 6H), 8.51 (d, J = 8.7 Hz, 3H), 7.77 (s, 3H), 7.75 (d, J = 8.7 Hz, 3H), 7.68 (d, J = 8.7 Hz, 6H), 3.09–2.99 (m, 6H), 2.26–2.17 (m, 6H), 1.00–0.83 (m, 12H), 0.68–0.54 (m, 12H), 0.47 (t, J = 8.7 Hz, 18H). ^{13}C NMR (76 MHz, CDCl_3): δ 154.57, 150.29, 148.28, 146.28, 141.17, 138.00, 136.17, 125.32, 125.24, 121.57, 120.54, 55.97, 36.78, 26.60, 22.86, 13.85. HRMS: found: 910.6043; calculated: 909.5961.

TruxNaph Self-Assembly

A mixture of **Trux3Pyr** (10 mg, 11 μmol , 2 equivalents) and the **RuNaph** complex (15.78 mg, 16.5 μmol , 3 equivalents) in methanol (2 mL) was stirred overnight at 50 °C. Then, diethyl ether (5 mL) was added, and the resulting suspension was centrifuged and washed two times with diethyl ether to give **TruxNaph** (21 mg, 4.5 μmol , 81%) as a dark solid. ^1H NMR (300 MHz, MeOD): δ 8.47 (d, J = 6.3 Hz, 12H), 8.33 (d, J = 8.4 Hz, 6H), 7.83 (d, J = 6.3 Hz, 12H), 7.79 (m, 12H), 7.30 (s, 12H), 5.87 (d, J = 6.1 Hz, 12H), 5.64 (d, J = 6.1 Hz, 12H), 2.91–2.82 (m, 12H), 2.54–2.44 (m, 12H), 2.13 (s, 18H), 1.99–2.08 (m, 12H), 1.37 (d, J = 6.9 Hz, 36H), 0.86–0.74 (m, 12H), 0.48–0.03 (m, 30H), 0.35 (t, J = 7.3 Hz, 18H), -0.14 (t, J = 7.0 Hz, 18H), -0.24 –(-0.34) (m, 6H). ^1H DOSY NMR (300 MHz, MeOD) $D = 2.99 \times 10^{-10} \text{ m}^2 \cdot \text{s}^{-1}$. FTICR-HRMS (m/z), [**TruxNaph-3TfO**] $^{3+}$: found: 1415.38771; calculated 1415.38762, [**TruxNaph-4TfO**] $^{4+}$: found: 1024.30249; calculated 1024.30257, [**TruxNaph-5TfO**] $^{5+}$: found: 789.65157; calculated 789.65155.

TruxTetra Self-Assembly

A mixture of **Trux3Pyr** (13 mg, 14.3 μmol , 2 equivalents) and the **RuTetra** complex (22.66 mg, 21.4 μmol , 3 equivalents) in methanol (2.5 mL) was stirred overnight at 50 °C. Then, diethyl ether (5 mL) was added, and the resulting suspension was centrifuged and washed two times with diethyl ether to give **TruxTetra** (22 mg, 4.4 μmol , 85%) as a dark solid. ^1H NMR (300 MHz, MeOD) δ 8.83–8.79 (m, 12H), 8.59 (d, J = 6.2 Hz, 12H), 8.21 (d, J = 8.4 Hz, 6H), 8.04–7.98 (m, 12H), 7.74 (d, J = 6.2 Hz, 12H), 7.68 (d, J = 8.4 Hz, 6H), 7.63 (s, 6H), 6.04–6.01 (m, 12H), 5.80–5.78 (m, 12H), 3.01–2.92 (m, 6H), 2.80–2.70 (m, 6H), 2.38–2.28 (m, 6H), 2.23 (s, 18H), 2.01–1.82 (m, 12H), 1.37 (d, J = 6.9 Hz, 36H), 0.85–0.64 (m, 12H), 0.30 (t, J = 7.3 Hz, 18H), 0.28–0.11 (m, 18H), 0.02–(-0.15) (m, 12H), -0.36 (t, J = 7.1 Hz, 18H), (-0.34) –(-0.40) (m, 6H). ^1H DOSY NMR (300 MHz, MeOD) $D = 2.85 \times 10^{-10} \text{ m}^2 \cdot \text{s}^{-1}$. FTICR-HRMS (m/z), [**TruxTetra-3TfO**] $^{3+}$: found: 1515.41921; calculated 1515.41892, [**TruxTetra-4TfO**] $^{4+}$: found: 1099.32576; calculated 1099.32605, [**TruxTetra-5TfO**] $^{5+}$: found: 849.67041; calculated 849.67033.

3.4. X-Ray Crystallographic Analysis

X-ray single-crystal diffraction data were collected at 150 K on an Agilent SuperNova diffractometer equipped with an Atlas CCD detector and micro-focus Cu $K\alpha$ radiation ($\lambda = 1.54184 \text{ \AA}$). The structures were solved by direct methods, expanded, and refined on F^2 by full matrix least-squares techniques by using *SHELX* (G.M. Sheldrick, 2008–2016) package. All non-hydrogen atoms were anisotropically refined, and the H atoms were included in the calculation without refinement. Multiscan empirical absorption was corrected with the *CrysAlisPro* program (*CrysAlisPro* 1.171.38.41r, Rigaku Oxford Diffraction, 2015).

The three structure refinements showed disordered electron density that could not be reliably modeled, and the program PLATON/SQUEEZE was used to remove the corresponding scattering contribution from the intensity data. This electron density can be attributed to solvent molecules (*n*-hexane for **Trux3pyr**, methanol for **TruxNaph** and **TruxTetra**) and missing triflate molecules (CF₃SO₃ anions for **TruxNaph** and **TruxTetra**). The assumed solvent composition and missing anion molecules were included in the calculation of the empirical formula, formula weight, density, linear absorption coefficient, and F(000).

Crystallographic data for **Trux3pyr**: C₁₃₈H₁₆₄N₆, M = 1906.75, colorless prism, 0.203 × 0.192 × 0.047 mm³, monoclinic, space group Pn, *a* = 11.7717(4) Å, *b* = 28.966(1) Å, *c* = 16.9134(4) Å, β = 91.318(2)°, *V* = 5765.6(3) Å³, *Z* = 2, ρ_{calc} = 1.098 g/cm³, μ = 0.470 mm⁻¹, F(000) = 2068, θ_{min} = 3.03°, θ_{max} = 76.65°, 25,637 reflections collected, 15,430 unique (R_{int} = 0.0459), parameters/restraints = 1247/4, R1 = 0.0759 and wR2 = 0.2084 using 12,872 reflections with I > 2σ(I), R1 = 0.0869 and wR2 = 0.2305 using all data, GOF = 1.058, absolute structure parameter = 0.1(8), -0.275 < Δρ < 0.454 e.Å⁻³. CCDC 1956952.

Crystallographic data for **TruxNaph**: C₂₆₈H₄₁₈F₁₈N₆O₇₀Ru₆S₆, M = 5984.84, black prism, 0.262 × 0.201 × 0.157 mm³, trigonal, space group P3₁21, *a* = 25.1943(5) Å, *b* = 25.1943(5) Å, *c* = 42.5843(7) Å, α = 90°, β = 90°, γ = 120°, *V* = 23409(1) Å³, *Z* = 3, ρ_{calc} = 1.274 g/cm³, μ = 3.364 mm⁻¹, F(000) = 9450, θ_{min} = 2.90°, θ_{max} = 72.812°, 124745 reflections collected, 30645 unique (R_{int} = 0.0277), parameters/restraints = 1107/45, R1 = 0.0503 and wR2 = 0.1546 using 15,980 reflections with I > 2σ(I), R1 = 0.0771 and wR2 = 0.1904 using all data, GOF = 0.945, absolute structure parameter = 0.447(9), -0.233 < Δρ < 0.200 e.Å⁻³. CCDC 1956951.

Crystallographic data for **TruxTetra**: C₂₉₂H₄₁₈F₁₈N₆O₇₀Ru₆S₆, M = 6273.10, black prism, 0.35 × 0.34 × 0.31 mm³, trigonal, space group P3₂21, *a* = 25.0842(6) Å, *b* = 25.0842(6) Å, *c* = 43.3591(10) Å, α = 90°, β = 90°, γ = 120°, *V* = 23627(1) Å³, *Z* = 3, ρ_{calc} = 1.323 g/cm³, μ = 3.360 mm⁻¹, F(000) = 9882, θ_{min} = 2.27°, θ_{max} = 72.88°, 1,250,008 reflections collected, 30,698 unique (R_{int} = 0.0493), parameters/restraints = 1203/39, R1 = 0.0605 and wR2 = 0.1777 using 19,178 reflections with I > 2σ(I), R1 = 0.0762 and wR2 = 0.1956 using all data, GOF = 0.965, absolute structure parameter = 0.204(7), -0.387 < Δρ < 0.469 e.Å⁻³. CCDC 1956958.

4. Conclusions

In summary, two metalla-cages were synthesized from a hexa-alkylated truxene ligand and hydroxyquinonato-bridged diruthenium complexes. While all starting components were achiral, the resulting **TruxNaph** and **TruxTetra** ruthenium based self-assemblies were chiral. Remarkably, only the homo-directional CC and AA enantiomers were observed in solution and in the solid state, an observation which is explained by the combination of the space filling between both facing alkylated truxene units and the tilt value of the lateral ruthenium panels. Work is now under progress to extend this approach toward interlocked supramolecular systems.

Supplementary Materials: The following are available online at <http://www.mdpi.com/2304-6740/8/1/1/s1>, NMR spectra, cif files and check cif files of **Trux3pyr**, **TruxNaph** and **TruxTetra**.

Author Contributions: M.S. and S.G. conceived the study, designed the experiments, analyzed the data, and wrote the paper; S.S., A.L., C.D. and A.B. performed the experiments; M.A. performed X-ray analyses; V.C. and F.A. performed ESI-FTICR analyses. All authors have read and agreed to the published version of the manuscript.

Funding: This research was funded by CNRS grant EMERGENCE@INC2019.

Acknowledgments: The authors gratefully acknowledge the MENRT for a PhD grant (S.S.) and RFI LUMOMAT for Postdoctoral fellow funding (A.B.). They also acknowledge the ASTRAL platform (SFR MATRIX, Univ. Angers) for their assistance in spectroscopic analyses. Finally, the financial support from the National FT-ICR network (FR 3624 CNRS) for conducting the research is gratefully acknowledged.

Conflicts of Interest: Authors declare no conflicts of interest.

References

1. Li, B.; He, T.; Fan, Y.; Yuan, X.; Qiu, H.; Yin, S. Recent developments in the construction of metallacycle/metallacage-cored supramolecular polymers via hierarchical self-assembly. *Chem. Commun.* **2019**, *55*, 8036–8059. [[CrossRef](#)] [[PubMed](#)]
2. Gan, M.-M.; Liu, J.-Q.; Zhang, L.; Wang, Y.-Y.; Hahn, F.E.; Han, Y.-F. Preparation and Post-Assembly Modification of Metallo-supramolecular Assemblies from Poly(*N*-Heterocyclic Carbene) Ligands. *Chem. Rev.* **2018**, *118*, 9587–9641. [[CrossRef](#)] [[PubMed](#)]
3. Lu, Y.; Zhang, H.-N.; Jin, G.-X. Molecular Borromean Rings Based on Half-Sandwich Organometallic Rectangles. *Acc. Chem. Res.* **2018**, *51*, 2148–2158. [[CrossRef](#)] [[PubMed](#)]
4. Roberts, D.A.; Pilgrim, B.S.; Nitschke, J.R. Covalent post-assembly modification in metallo-supramolecular chemistry. *Chem. Soc. Rev.* **2018**, *47*, 626–644. [[CrossRef](#)]
5. Wu, G.-Y.; Chen, L.-J.; Xu, L.; Zhao, X.-L.; Yang, H.-B. Construction of supramolecular hexagonal metallacycles via coordination-driven self-assembly: Structure, properties and application. *Coord. Chem. Rev.* **2018**, *369*, 39–75. [[CrossRef](#)]
6. Huang, S.-L.; Hor, T.S.A.; Jin, G.-X. Metallacyclic assembly of interlocked superstructures. *Coord. Chem. Rev.* **2017**, *333*, 1–26. [[CrossRef](#)]
7. Frank, M.; Johnstone, M.D.; Clever, G.H. Interpenetrated Cage Structures. *Chem. Eur. J.* **2016**, *22*, 14104–14125. [[CrossRef](#)]
8. Cook, T.R.; Stang, P.J. Recent Developments in the Preparation and Chemistry of Metallacycles and Metallacages via Coordination. *Chem. Rev.* **2015**, *115*, 7001–7045. [[CrossRef](#)]
9. Henkelis, J.J.; Hardie, M.J. Controlling the assembly of cyclotrimer-ethylene-derived coordination cages. *Chem. Commun.* **2015**, *51*, 11929–11943. [[CrossRef](#)]
10. Bilbeisi, R.A.; Olsen, J.-C.; Charbonnière, L.J.; Trabolsi, A. Self-assembled discrete metal–organic complexes: Recent advances. *Inorg. Chim. Acta* **2014**, *417*, 79–108. [[CrossRef](#)]
11. Mishra, A.; Gupta, R. Supramolecular architectures with pyridine-amide based ligands: Discrete molecular assemblies and their applications. *Dalton Trans.* **2014**, *43*, 7668–7682. [[CrossRef](#)] [[PubMed](#)]
12. Mukherjee, S.; Mukherjee, P.S. Template-free multicomponent coordination-driven self-assembly of Pd(II)/Pt(II) molecular cages. *Chem. Commun.* **2014**, *50*, 2239–2248. [[CrossRef](#)] [[PubMed](#)]
13. Thanasekaran, P.; Lee, C.-H.; Lu, K.-L. Neutral discrete metal–organic cyclic architectures: Opportunities for structural features and properties in confined spaces. *Coord. Chem. Rev.* **2014**, *280*, 96–175. [[CrossRef](#)]
14. Yoshizawa, M.; Klosterman, J.K. Molecular architectures of multi-anthracene assemblies. *Chem. Soc. Rev.* **2014**, *43*, 1885–1898. [[CrossRef](#)] [[PubMed](#)]
15. Mishra, A.; Kang, S.C.; Chi, K.-W. Coordination-Driven Self-Assembly of Arene–Ruthenium Compounds. *Eur. J. Inorg. Chem.* **2013**, *2013*, 5222–5232. [[CrossRef](#)]
16. Ward, M.D.; Raithby, P.R. Functional behaviour from controlled self-assembly: Challenges and prospects. *Chem. Soc. Rev.* **2013**, *42*, 1619–1636. [[CrossRef](#)] [[PubMed](#)]
17. Chakrabarty, R.; Mukherjee, P.S.; Stang, P.J. Supramolecular coordination: Self-assembly of finite two- and three-dimensional ensembles. *Chem. Rev.* **2011**, *111*, 6810–6918. [[CrossRef](#)]
18. Wang, Y.-X.; Zhou, Q.-F.; Jiang, S.-T.; Zhang, Y.; Yin, G.-Q.; Jiang, B.; Li, X.; Tan, H.; Yang, H.-B. Photoresponsive Chirality-Tunable Supramolecular Metallacycles. *Macromol. Rapid Commun.* **2018**, *39*, 1800454. [[CrossRef](#)]
19. Diaz-Moscoso, A.; Ballester, P. Light-responsive molecular containers. *Chem. Commun.* **2017**, *53*, 4635–4652. [[CrossRef](#)]
20. Saha, M.L.; Yan, X.; Stang, P.J. Photophysical Properties of Organoplatinum(II) Compounds and Derived Self-Assembled Metallacycles and Metallacages: Fluorescence and its Applications. *Acc. Chem. Res.* **2016**, *49*, 2527–2539. [[CrossRef](#)]
21. Qu, D.-H.; Wang, Q.-C.; Zhang, Q.-W.; Ma, X.; Tian, H. Photoresponsive Host–Guest Functional Systems. *Chem. Rev.* **2015**, *115*, 7543–7588. [[CrossRef](#)] [[PubMed](#)]
22. Zarra, S.; Wood, D.M.; Roberts, D.A.; Nitschke, J.R. Molecular containers in complex chemical systems. *Chem. Soc. Rev.* **2015**, *44*, 419–432. [[CrossRef](#)] [[PubMed](#)]
23. Krykun, S.; Dekhtiarenko, M.; Canevet, D.; Carre, V.; Aubriet, F.; Levillain, E.; Allain, M.; Voitenko, Z.; Sallé, M.; Goeb, S. Metalla-Assembled Electron-Rich Tweezers: Redox-Controlled Guest Release Through Supramolecular Dimerization. *Angew. Chem. Int. Ed.* **2019**. [[CrossRef](#)] [[PubMed](#)]

24. Plessius, R.; Orth, N.; Ivanović-Burmazović, I.; Siegler, M.A.; Reek, J.N.H.; van der Vlugt, J.I. Reversible multi-electron storage in dual-site redox-active supramolecular cages. *Chem. Commun.* **2019**, *55*, 12619–12622. [[CrossRef](#)] [[PubMed](#)]
25. Szalóki, G.; Krykun, S.; Croué, V.; Allain, M.; Morille, Y.; Aubriet, F.; Carré, V.; Voitenko, Z.; Goeb, S.; Sallé, M. Redox-Driven Transformation of a Discrete Molecular Cage into an Infinite 3D Coordination Polymer. *Chem. Eur. J.* **2018**, *24*, 11273–11277. [[CrossRef](#)]
26. Szalóki, G.; Croué, V.; Carré, V.; Aubriet, F.; Alévêque, O.; Levillain, E.; Allain, M.; Arago, J.; Orti, E.; Goeb, S.; et al. Controlling the Host-Guest Interaction Mode through a Redox Stimulus. *Angew. Chem. Int. Ed.* **2017**, *56*, 16272–16276. [[CrossRef](#)]
27. Croué, V.; Goeb, S.; Szalóki, G.; Allain, M.; Sallé, M. Reversible Guest Uptake/Release by Redox-Controlled Assembly/Disassembly of a Coordination Cage. *Angew. Chem. Int. Ed.* **2016**, *55*, 1746–1750. [[CrossRef](#)]
28. Croué, V.; Goeb, S.; Sallé, M. Metal-driven self-assembly: The case of redox-active discrete architectures. *Chem. Commun.* **2015**, *51*, 7275–7289. [[CrossRef](#)]
29. Xu, L.; Wang, Y.X.; Chen, L.J.; Yang, H.B. Construction of multiferrocenyl metallacycles and metallacages via coordination-driven self-assembly: From structure to functions. *Chem. Soc. Rev.* **2015**, *44*, 2148–2167. [[CrossRef](#)]
30. Bivaud, S.; Goeb, S.; Croué, V.; Dron, P.I.; Allain, M.; Sallé, M. Self-Assembled Containers Based on Extended Tetrathiafulvalene. *J. Am. Chem. Soc.* **2013**, *135*, 10018–10021. [[CrossRef](#)]
31. Bivaud, S.; Balandier, J.Y.; Chas, M.; Allain, M.; Goeb, S.; Sallé, M. A Metal-Directed Self-Assembled Electroactive Cage with Bis(pyrrolo)tetrathiafulvalene (BPTTF) Side Walls. *J. Am. Chem. Soc.* **2012**, *134*, 11968–11970. [[CrossRef](#)] [[PubMed](#)]
32. Chen, L.; Chen, Q.; Wu, M.; Jiang, F.; Hong, M. Controllable Coordination-Driven Self-Assembly: From Discrete Metallogages to Infinite Cage-Based Frameworks. *Acc. Chem. Res.* **2015**, *48*, 201–210. [[CrossRef](#)] [[PubMed](#)]
33. Chen, L.-J.; Yang, H.-B. Construction of Stimuli-Responsive Functional Materials via Hierarchical Self-Assembly Involving Coordination Interactions. *Acc. Chem. Res.* **2018**, *51*, 2699–2710. [[CrossRef](#)] [[PubMed](#)]
34. Kim, T.Y.; Vasdev, R.A.S.; Preston, D.; Crowley, J.D. Strategies for Reversible Guest Uptake and Release from Metallosupramolecular Architectures. *Chem. Eur. J.* **2018**, *24*, 14878–14890. [[CrossRef](#)] [[PubMed](#)]
35. Casini, A.; Woods, B.; Wenzel, M. The Promise of Self-Assembled 3D Supramolecular Coordination Complexes for Biomedical Applications. *Inorg. Chem.* **2017**, *56*, 14715–14729. [[CrossRef](#)]
36. Ahmad, N.; Younus, H.A.; Chughtai, A.H.; Verpoort, F. Metal-organic molecular cages: Applications of biochemical implications. *Chem. Soc. Rev.* **2015**, *44*, 9–25. [[CrossRef](#)]
37. McConnell, A.J.; Wood, C.S.; Neelakandan, P.P.; Nitschke, J.R. Stimuli-Responsive Metal-Ligand Assemblies. *Chem. Rev.* **2015**, *115*, 7729–7793. [[CrossRef](#)]
38. Xu, L.; Wang, Y.-X.; Yang, H.-B. Recent advances in the construction of fluorescent metallogages and metallogages via coordination-driven self-assembly. *Dalton Trans.* **2015**, *44*, 867–890. [[CrossRef](#)]
39. Therrien, B. Discrete Metalla-Assemblies as Drug Delivery Vectors. In *Nanomaterials in Drug Delivery, Imaging, and Tissue Engineering*; John Wiley & Sons, Inc.: New York, NY, USA, 2013; pp. 145–166. [[CrossRef](#)]
40. Amouri, H.; Desmarets, C.; Moussa, J. Confined Nanospaces in Metallogages: Guest Molecules, Weakly Encapsulated Anions, and Catalyst Sequestration. *Chem. Rev.* **2012**, *112*, 2015–2041. [[CrossRef](#)]
41. Therrien, B. Drug Delivery by Water-Soluble Organometallic Cages. In *Chemistry of Nanocontainers*; Albrecht, M., Hahn, E., Eds.; Springer: Berlin/Heidelberg, Germany, 2012; Volume 319, pp. 35–55.
42. Chen, L.-J.; Zhu, J.-L.; Yang, H.-B. CHAPTER 4 Self-assembled Chiral Metallomacrocycles. In *Metallomacrocycles: From Structures to Applications*; The Royal Society of Chemistry: London, UK, 2019; pp. 77–105. [[CrossRef](#)]
43. Chen, L.-J.; Yang, H.-B.; Shionoya, M. Chiral metallosupramolecular architectures. *Chem. Soc. Rev.* **2017**, *46*, 2555–2576. [[CrossRef](#)]
44. Jędrzejewska, H.; Szumna, A. Making a Right or Left Choice: Chiral Self-Sorting as a Tool for the Formation of Discrete Complex Structures. *Chem. Rev.* **2017**, *117*, 4863–4899. [[CrossRef](#)] [[PubMed](#)]
45. Liu, M.; Zhang, L.; Wang, T. Supramolecular Chirality in Self-Assembled Systems. *Chem. Rev.* **2015**, *115*, 7304–7397. [[CrossRef](#)] [[PubMed](#)]
46. Castilla, A.M.; Ramsay, W.J.; Nitschke, J.R. Stereochemistry in Subcomponent Self-Assembly. *Acc. Chem. Res.* **2014**, *47*, 2063–2073. [[CrossRef](#)] [[PubMed](#)]

47. Bloch, W.M.; Clever, G.H. Integrative self-sorting of coordination cages based on 'naked' metal ions. *Chem. Commun.* **2017**, *53*, 8506–8516. [[CrossRef](#)]
48. He, Z.; Jiang, W.; Schalley, C.A. Integrative self-sorting: A versatile strategy for the construction of complex supramolecular architecture. *Chem. Soc. Rev.* **2015**, *44*, 779–789. [[CrossRef](#)]
49. Safont-Sempere, M.M.; Fernández, G.; Würthner, F. Self-Sorting Phenomena in Complex Supramolecular Systems. *Chem. Rev.* **2011**, *111*, 5784–5814. [[CrossRef](#)]
50. Schulte, T.R.; Holstein, J.J.; Clever, G.H. Chiral Self-Discrimination and Guest Recognition in Helicene-Based Coordination Cages. *Angew. Chem. Int. Ed.* **2019**, *58*, 5562–5566. [[CrossRef](#)]
51. Beaudoin, D.; Rominger, F.; Mastalerz, M. Chiral Self-Sorting of [2 + 3] Salicylimine Cage Compounds. *Angew. Chem. Int. Ed.* **2017**, *56*, 1244–1248. [[CrossRef](#)]
52. Rota Martir, D.; Escudero, D.; Jacquemin, D.; Cordes, D.B.; Slawin, A.M.Z.; Fruchtl, H.A.; Warriner, S.L.; Zysman-Colman, E. Homochiral Emissive Λ^8 - and Δ^8 -[Ir₃Pd₄]¹⁶⁺ Supramolecular Cages. *Chem. Eur. J.* **2017**, *23*, 14358–14366. [[CrossRef](#)]
53. Boer, S.A.; Turner, D.R. Self-selecting homochiral quadruple-stranded helicates and control of supramolecular chirality. *Chem. Commun.* **2015**, *51*, 17375–17378. [[CrossRef](#)]
54. Maeda, C.; Kamada, T.; Aratani, N.; Osuka, A. Chiral self-discriminative self-assembly of meso–meso linked diporphyrins. *Coord. Chem. Rev.* **2007**, *251*, 2743–2752. [[CrossRef](#)]
55. Lützen, A.; Hapke, M.; Griep-Raming, J.; Haase, D.; Saak, W. Synthesis and Stereoselective Self-Assembly of Double- and Triple-Stranded Helicates. *Angew. Chem. Int. Ed.* **2002**, *41*, 2086–2089. [[CrossRef](#)]
56. Masood, M.A.; Enemark, E.J.; Stack, T.D.P. Ligand Self-Recognition in the Self-Assembly of a [Cu(L)]₂²⁺ Complex: The Role of Chirality. *Angew. Chem. Int. Ed.* **1998**, *37*, 928–932. [[CrossRef](#)]
57. Arribas, C.S.; Wendt, O.F.; Sundin, A.P.; Carling, C.-J.; Wang, R.; Lemieux, R.P.; Wärnmark, K. Formation of an heterochiral supramolecular cage by diastereomer self-discrimination: Fluorescence enhancement and C60 sensing. *Chem. Commun.* **2010**, *46*, 4381–4383. [[CrossRef](#)]
58. Weilandt, T.; Kiehne, U.; Schnakenburg, G.; Lützen, A. Diastereoselective self-assembly of dinuclear heterochiral metallocsupramolecular rhombs in a self-discriminating process. *Chem. Commun.* **2009**, *17*, 2320–2322. [[CrossRef](#)]
59. Zhang, D.; Ronson, T.K.; Greenfield, J.L.; Brotin, T.; Berthault, P.; Léonce, E.; Zhu, J.-L.; Xu, L.; Nitschke, J.R. Enantiopure [Cs⁺/XeC]Cryptophane]cFeII4L4 Hierarchical Superstructures. *J. Am. Chem. Soc.* **2019**, *141*, 8339–8345. [[CrossRef](#)]
60. Zhang, P.; Wang, X.; Xuan, W.; Peng, P.; Li, Z.; Lu, R.; Wu, S.; Tian, Z.; Cao, X. Chiral separation and characterization of triazatruxene-based face-rotating polyhedra: The role of non-covalent facial interactions. *Chem. Commun.* **2018**, *54*, 4685–4688. [[CrossRef](#)]
61. Qu, H.; Tang, X.; Wang, X.; Li, Z.; Huang, Z.; Zhang, H.; Tian, Z.; Cao, X. Chiral molecular face-rotating sandwich structures constructed through restricting the phenyl flipping of tetraphenylethylene. *Chem. Sci.* **2018**, *9*, 8814–8818. [[CrossRef](#)]
62. Wang, Y.; Fang, H.; Tranca, I.; Qu, H.; Wang, X.; Markvoort, A.J.; Tian, Z.; Cao, X. Elucidation of the origin of chiral amplification in discrete molecular polyhedra. *Nat. Commun.* **2018**, *9*, 488. [[CrossRef](#)]
63. Wang, X.; Peng, P.; Xuan, W.; Wang, Y.; Zhuang, Y.; Tian, Z.; Cao, X. Narcissistic chiral self-sorting of molecular face-rotating polyhedra. *Org. Biomol. Chem.* **2018**, *16*, 34–37. [[CrossRef](#)]
64. Wang, Y.; Fang, H.; Zhang, W.; Zhuang, Y.; Tian, Z.; Cao, X. Interconversion of molecular face-rotating polyhedra through turning inside out. *Chem. Commun.* **2017**, *53*, 8956–8959. [[CrossRef](#)] [[PubMed](#)]
65. Wang, X.; Wang, Y.; Yang, H.; Fang, H.; Chen, R.; Sun, Y.; Zheng, N.; Tan, K.; Lu, X.; Tian, Z.; et al. Assembled molecular face-rotating polyhedra to transfer chirality from two to three dimensions. *Nat. Commun.* **2016**, *7*, 12469. [[CrossRef](#)] [[PubMed](#)]
66. Bols, P.S.; Anderson, H.L. Shadow Mask Templates for Site-Selective Metal Exchange in Magnesium Porphyrin Nanorings. *Angew. Chem. Int. Ed.* **2018**, *57*, 7874–7877. [[CrossRef](#)] [[PubMed](#)]
67. Tehfe, M.-A.; Lalevée, J.; Telitel, S.; Contal, E.; Dumur, F.; Gimes, D.; Bertin, D.; Nechab, M.; Graff, B.; Morlet-Savary, F.; et al. Polyaromatic Structures as Organo-Photoinitiator Catalysts for Efficient Visible Light Induced Dual Radical/Cationic Photopolymerization and Interpenetrated Polymer Networks Synthesis. *Macromolecules* **2012**, *45*, 4454–4460. [[CrossRef](#)]

68. Kanibolotsky, A.L.; Berridge, R.; Skabara, P.J.; Perepichka, I.F.; Bradley, D.D.C.; Koeberg, M. Synthesis and Properties of Monodisperse Oligofluorene-Functionalized Truxenes: Highly Fluorescent Star-Shaped Architectures. *J. Am. Chem. Soc.* **2004**, *126*, 13695–13702. [[CrossRef](#)]
69. Guan, J.; Xu, F.; Tian, C.; Pu, L.; Yuan, M.-S.; Wang, J. Tricolor Luminescence Switching by Thermal and Mechanical Stimuli in the Crystal Polymorphs of Pyridyl-substituted Fluorene. *Chem. Asian J.* **2019**, *14*, 216–222. [[CrossRef](#)]
70. Therrien, B. Arene Ruthenium Cages: Boxes Full of Surprises. *Eur. J. Inorg. Chem.* **2009**, *17*, 2445–2453. [[CrossRef](#)]
71. Cohen, Y.; Avram, L.; Frish, L. Diffusion NMR Spectroscopy in Supramolecular and Combinatorial Chemistry: An Old Parameter-New Insights. *Angew. Chem. Int. Ed.* **2005**, *44*, 520–554. [[CrossRef](#)]
72. Kim, T.; Singh, N.; Oh, J.; Kim, E.-H.; Jung, J.; Kim, H.; Chi, K.-W. Selective Synthesis of Molecular Borromean Rings: Engineering of Supramolecular Topology via Coordination-Driven Self-Assembly. *J. Am. Chem. Soc.* **2016**, *138*, 8368–8371. [[CrossRef](#)]
73. Fazio, E.; Haynes, C.J.E.; de la Torre, G.; Nitschke, J.R.; Torres, T. A giant M_2L_3 metallo-organic helicate based on phthalocyanines as a host for electroactive molecules. *Chem. Commun.* **2018**, *54*, 2651–2654. [[CrossRef](#)]
74. García-Frutos, E.M.; Gómez-Lor, B.; Monge, Á.; Gutiérrez-Puebla, E.; Alkorta, I.; Elguero, J. Synthesis and Preferred All-syn Conformation of C3-Symmetrical N-(Hetero)arylmethyl Triindoles. *Chem. Eur. J.* **2008**, *14*, 8555–8561. [[CrossRef](#)] [[PubMed](#)]
75. Mirtschin, S.; Slabon-Turski, A.; Scopelliti, R.; Velders, A.H.; Severin, K. A Coordination Cage with an Adaptable Cavity Size. *J. Am. Chem. Soc.* **2010**, *132*, 14004–14005. [[CrossRef](#)] [[PubMed](#)]
76. Govindaswamy, P.; Linder, D.; Lacour, J.; Süß-Fink, G.; Therrien, B. Self-assembled hexanuclear arene ruthenium metallo-prisms with unexpected double helical chirality. *Chem. Commun.* **2006**, *45*, 4691–4693. [[CrossRef](#)] [[PubMed](#)]
77. Bailar, J.C. Some problems in the stereochemistry of coordination compounds: Introductory lecture. *J. Inorg. Nucl. Chem.* **1958**, *8*, 165–175. [[CrossRef](#)]
78. Barry, N.P.E.; Furrer, J.; Therrien, B. In- and Out-of-Cavity Interactions by Modulating the Size of Ruthenium Metallarectangles. *Helv. Chim. Acta* **2010**, *93*, 1313–1328. [[CrossRef](#)]



© 2019 by the authors. Licensee MDPI, Basel, Switzerland. This article is an open access article distributed under the terms and conditions of the Creative Commons Attribution (CC BY) license (<http://creativecommons.org/licenses/by/4.0/>).